Atmos. Meas. Tech., 8, 2577–2588, 2015
www.atmos-meas-tech.net/8/2577/2015/
doi:10.5194/amt-8-2577-2015

Atmospheric Measurement Techniques
Open Access

The charging of neutral dimethylamine and dimethylamine–sulfuric acid clusters using protonated acetone

K. Ruusuvuori[1], P. Hietala[1], O. Kupiainen-Määttä[1], T. Jokinen[1], H. Junninen[1], M. Sipilä[1], T. Kurtén[2], and H. Vehkamäki[1]

[1]Division of Atmospheric Sciences, Department of Physics, P.O. Box 64, 00014 University of Helsinki, Helsinki, Finland
[2]Laboratory of Physical Chemistry, Department of Chemistry, University of Helsinki, P.O. Box 55, 00014, Helsinki, Finland

Correspondence to: K. Ruusuvuori (kai.ruusuvuori@helsinki.fi)

Received: 21 August 2014 – Published in Atmos. Meas. Tech. Discuss.: 6 November 2014
Revised: 16 April 2015 – Accepted: 29 May 2015 – Published: 25 June 2015

Abstract. Sulfuric acid is generally considered one of the most important substances taking part in atmospheric particle formation. However, in typical atmospheric conditions in the lower troposphere, sulfuric acid and water alone are unable to form particles. It has been suggested that strong bases may stabilize sulfuric acid clusters so that particle formation may occur. More to the point, amines – strong organic bases – have become the subject of interest as possible cause for such stabilization. To probe whether amines play a role in atmospheric nucleation, we need to be able to measure accurately the gas-phase amine vapour concentration. Such measurements often include charging the neutral molecules and molecular clusters in the sample. Since amines are bases, the charging process should introduce a positive charge. This can be achieved by, for example, using chemical ionization with a positively charged reagent with a suitable proton affinity. In our study, we have used quantum chemical methods combined with a cluster dynamics code to study the use of acetone as a reagent ion in chemical ionization and compared the results with measurements performed with a chemical ionization atmospheric pressure interface time-of-flight mass spectrometer (CI-APi-TOF). The computational results indicate that protonated acetone is an effective reagent in chemical ionization. However, in the experiments the reagent ions were not depleted at the predicted dimethylamine concentrations, indicating that either the modelling scheme or the experimental results – or both – contain unidentified sources of error.

1 Introduction

The formation of molecular clusters from trace gases is an important process in the atmosphere. It has been observed in practice everywhere where it has been experimentally investigated (Zhang et al., 2012; Kulmala et al., 2013; Kyrö et al., 2013). While the initial steps of atmospheric particle formation generally require sulfuric acid (SA, Sipilä et al., 2010), it cannot on its own, or even with water, form clusters that are stable enough in typical atmospheric conditions in the lower troposphere. This means that for particle formation and subsequent growth to happen, one or more other condensing vapours are needed. Strong bases such as amines could stabilize the sulfuric acid containing clusters enough to let growth occur. The role of amines in new particle formation has been the subject of recent studies, and it has been suggested that they may indeed play an important role, at least in the lower atmosphere (Almeida et al., 2013; Petäjä et al., 2011). It has been shown experimentally that even sub-ppt concentrations of dimethylamine (DMA) significantly enhance the formation of clusters containing sulfuric acid (Almeida et al., 2013). DMA, however, is not usually as abundant in the atmosphere as for example ammonia. Thus, more measurement data are needed to conclude to what extent atmospheric particle formation is assisted by amines such as DMA.

In order to interpret measurement data, thorough understanding of what is actually taking place in a measurement is needed. Since electric fields can be used to manipulate the trajectories of ions, and ions can readily be detected, a common approach for measuring neutral gas-phase molecules

and clusters is to first ionize them and then detect the ions. This process of charging imposes a whole new layer of problems and questions on a measurement, such as the following: how big a fraction of the molecules and clusters within a sample will end up getting charged, will the charging process charge only certain types of clusters, will the charging process cause clusters to break up or evaporate molecules, and how will the charged clusters behave after they have been charged but before they are detected? One widely used method of charging is chemical ionization (CI), used in, for example, chemical ionization mass spectrometers (CIMS). Since amines are bases, the sample air needs to be positively charged in amine measurements. In selective positive ion chemical ionization, a reagent with a suitable proton affinity is first charged, and then used to charge the molecules with a higher proton affinity than the reagent. The advantages of this method are that the proton transfer reaction is not in itself violent enough to break clusters apart (although the charged cluster may become unstable after receiving the charge) and that bases have high proton affinities. Thus, by choosing a reagent with a high proton affinity (but lower than that of the base we wish to detect), we can avoid charging most of the compounds with a lower proton affinity. The disadvantage is that if there are high enough concentrations of bases in the sample with an even higher proton affinity than the molecule species we wish to detect, these molecules may end up receiving most of the charge. CI mass spectrometry is not the only measurement technique that takes advantage of different proton affinities. For example, a similar approach to charging is used also in ion mobility spectrometry (IMS) with doped gases (Puton et al., 2008).

Comparing the proton affinities of two free molecules may give a qualitative answer regarding the fate of the proton when one of these two molecules is protonated and the molecules collide. However, for a full understanding of the process, a more detailed description is needed. When the two molecules collide, they will likely first form a cluster, after which the formed cluster will evaporate into two monomers within some period of time, the length of which depends on the stability of the cluster. When the cluster evaporates, it is likely that the molecule with a higher proton affinity (i.e. the stronger base) will retain the proton, but the fate of the proton might also depend on the structure of the cluster. Assigning the proton to either molecule within the cluster may not be straightforward. Due to thermal vibrations, the proton may, for example, spend 10 % of the time closer to one of the molecules and 90 % of the time closer to the other molecule (Loukonen et al., 2014).

If the neutral collision partner is not a single base molecule but instead a cluster containing that molecule, further complications arise. The proton affinity of a cluster may not give even a qualitatively correct description of the result. Once the collision has happened and a cluster has been formed, the first molecule to break off from the cluster is most probably the one that is most loosely bound and has the highest evaporation rate. For instance, if the initial neutral cluster consists of one base molecule and one acid molecule, this acid molecule is likely to evaporate rapidly after the collision with the protonated base molecule. After this, the situation is as if the neutral collision partner had been the plain base molecule. This is why the proton affinity of the neutral base molecule, not the whole cluster, should be used as an indicator of the success of the charging. However, the structure and composition of the cluster may still affect the proton transfer. For example if the neutral molecule is hydrated, the proton transfer reaction may happen through a water bridge instead of direct proton transfer from acid to base. On the other hand, if the neutral molecule has clustered with acidic molecules, a proton transfer reaction may have already happened.

The use of acetone and ethanol as ionization reagents in CIMS measurements has recently been studied by Yu and Lee (2012). Although in their CIMS measurements ethanol provided a better sensitivity and limit of detection than acetone, the higher proton affinity of acetone makes it an interesting option due to its higher selectivity to strong bases.

Our aim is to study computationally the use of protonated (H^+) acetone (Ac) dimers for charging (and subsequently detecting) DMA molecules and DMA–SA clusters. The modelling results will also be compared with measurement data. Understanding the possible reaction pathways as well as comparing predictions with measurements will give us important insight on amine measurements performed using an acetone-based chemical ionization atmospheric pressure interface time-of-flight mass spectrometer (CI-APi-TOF).

2 Methods

Quantum chemical calculations of structures and frequencies were performed using the quantum chemistry program suites Gaussian 09 (Frisch et al., 2009) and Turbomole versions 6.3.1 and 6.5 (Ahlrichs et al., 1989). Geometries, standard enthalpies (at 298.15 K and 1 atm), Gibbs free energies of formation and evaporation rates for clusters are obtained as described in the paper by Ortega et al. (2012). The quantum chemical results were used as input in our cluster dynamics code ACDC (see Kupiainen-Määttä et al., 2013, and references therein), which was employed to model the cluster distributions before, during and after charging.

In addition to the quantum chemical data, the ACDC code requires several input parameters specifying the conditions under study. The temperature was set to 298.15 K in all simulations. In the first set of simulations, the concentration of sulfuric acid molecules was given three different values: 0, 10^6 and 10^8 cm^{-3}. Sulfuric acid was included due to its role in the atmosphere and the fact that it was present in the ambient air used for dilution in the measurements. The concentration of neutral dimethylamine molecules was also given three different values: 0.01, 100 and 3000 ppt. This first set of simulations was used to study the time evolution of the cluster

concentrations as well as the effect of sulfuric acid concentration. In the second set of simulations, the SA concentration 10^7 cm^{-3} was also included, and the DMA concentration was given several values between 0.01 and 3000 ppt to allow comparison with experimental data. In the ACDC simulations, the first step is to solve the steady-state distribution of neutral clusters, resulting in a cluster distribution containing monomers as well as clusters with one SA and one DMA. The given SA and DMA concentrations are a sum of the free monomers and the molecules found in the $(SA)_1(DMA)_1$ clusters. Next, the neutral clusters are mixed with the charger ions. The time given for the charging was set to 0.2 s. This parameter was also tested for sensitivity by using also values 0.01, 0.1, 0.15, 0.25, 0.3 and 0.4 s. The concentration of charger ions was initially set to 10^6 cm^{-3}. The ratio between protonated acetone monomers and protonated acetone dimers was set to be the same as was observed in the measurements, resulting in 20 % of the total amount being protonated acetone monomers. Also the number of charger ions was tested for sensitivity using values as high as 10^{12} cm^{-3}. It should be noted that this high charger ion concentrations are in practice very hard to achieve, and the use of such high values has been done purely to test the sensitivity of the simulation. The concentration of neutral acetone monomers was initially set to 0 cm^{-3}, but values of 10^6 and 10^9 cm^{-3} were also tested. Furthermore, the use of only protonated acetone monomers as well as only protonated acetone dimers was also tested.

In the ACDC code, the charging process is not modelled using the proton affinities of the molecules and clusters, but by simulating the process explicitly: a collision with an ion always leads to the formation of a cluster, the cluster will evaporate according to the evaporation rates calculated from the Gibbs formation free energies of the cluster, and the way the molecules are arranged in the cluster does not affect the outcome of the collision (it only affects the Gibbs free energies). Neutral-neutral collision rates are determined using classical gas kinetics, and ion-neutral collision rates are calculated using the parameterization by Su and Chesnavich (1982). As a product of the simulations, we also obtain fluxes to and from different cluster sizes. This information was used to identify the dominant reaction paths leading to the formation and loss of the allowed cluster types.

The maximum size of the clusters the ACDC is modelling varies with the charging state of the cluster. Neutral clusters that grow to $(SA)_2(DMA)_1$ or larger sizes by the addition of SA or DMA are assumed to become stable clusters and grow irreversibly out of the system, while for positively charged clusters the limit is the $H^+(SA)_2(DMA)_3$ cluster that is known to be stable. Any cluster as big as this would, however, be unlikely to have time to form inside the instrument, as the timescale of SA collisions with clusters even at $[SA] = 10^8$ cm^{-3} is on the order of 10 s or more. All clusters included in the simulations are listed in Table 1. For clusters larger than these – with the exception of the aforementioned clusters, which are assumed to irreversibly grow out of the system – there are no quantum chemical data yet available, which means their stability is unknown. Thus, clusters that grow beyond these size limits are brought back into the system by evaporating monomers. The evaporated molecules are determined based on how many acids and bases the cluster contains and which of these acids and bases are the weakest. In other words, if the cluster has more acid (base) molecules than base (acid) molecules, an acid (base) molecule will evaporate with the weakest acid (base) molecule leaving first.

Table 1. Cluster size limits for clusters. If the clusters grow to larger sizes, they will be brought within the system boundaries by evaporating monomers.

Charging state	Composition	Number of molecules			
		SA	Ac	DMA	H^+
Neutral					
	Pure SA	1	0	0	0
	Clusters with DMA	0–1	0	1	0
	Clusters with Ac	0–1	1	0	0
		0	1	1	0
Positive					
	With DMA	0–1	0	1	1
		0–1	0	2	1
		0–1	0	3	1
	With Ac	0	1	0	1
		0–1	2	0	1
		0	3	0	1
	With Ac and DMA	0–1	1	1	1
		0-1	2	1	1
		0	1	2	1

The measurements were performed in the Hyytiälä field station SMEAR II using CI-APi-TOF (see Jokinen et al., 2012, and references therein) in order to test its performance in measuring DMA using protonated acetone as an ionization reagent. The instrument was deployed in the positive ion mode. Acetone was introduced in the sheath air (total flow of ~ 20 L min^{-1}) using a bubbler with a flow of clean pressurized air through it (acetone flow of 1 L min^{-1}) or using a pulse-free HPLC piston pump (acetone flow of 2 µL min^{-1}). The measurements did not measure ambient concentrations of DMA. Instead, DMA was obtained from a commercially available permeation tube, for which the manufacturer (VICI) promises a standard permeation rate of 12 ng minm$^{-1} \pm 50$ % at 40 °C. A commercially available gas calibrator (Ansyco Sycos Kt-PM2) was used for permeation. The gas calibrator consists of a temperature-controlled oven for the permeation tube and a gas dilution system with mass flow controllers. The resulting DMA standard gas was then further diluted using ambient air. The DMA concentration was varied by adjusting the level of dilution from 10 to 50 L min^{-1}. Although a separate collision dissociation cham-

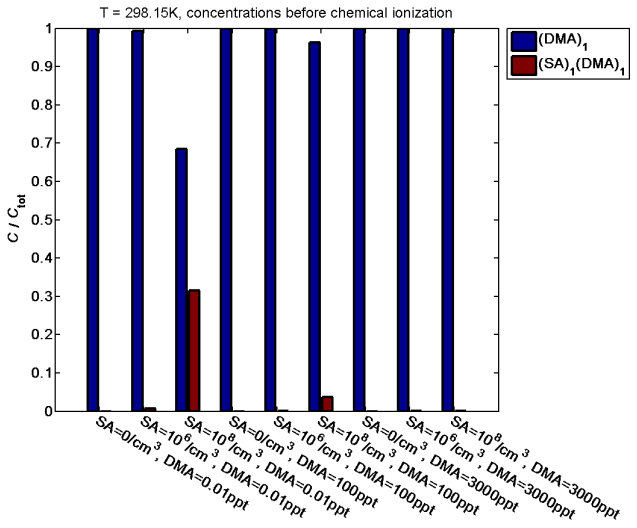

Figure 1. Relative concentrations before chemical ionization.

ber (CDC) is not used in the CI-APi-TOF, fragmentation occurs as the charged sample passes through the APi. Due to the complexity of the CI-APi-TOF, it is not possible to say to which CDC collision energy the fragmentation would correspond. However, during all measurements the fragmentation level was kept as small as possible through voltage tuning of the ion optics so that the voltage differences in the APi are minimized.

3 Model results

Concentrating first on the ACDC modelling results, Fig. 1 shows the relative steady-state concentrations of neutral DMA-containing species before the ionization for different concentrations of SA and DMA. Before chemical ionization, DMA is present mostly as monomers regardless of the SA or DMA concentration. Clusters with one DMA and one SA molecule appear when the SA concentration is 10^6 or $10^8\,\mathrm{cm}^{-3}$. The fraction of DMA bound to these SA–DMA clusters depends somewhat on the SA and DMA concentration, being less than 5 % for [DMA] = 100 ppt and $\sim 30\,\%$ for [DMA] = 0.01 ppt when $[\mathrm{SA}] = 10^8\,\mathrm{cm}^{-3}$, and less than 1 % for [DMA] = 0.01 ppt when $[\mathrm{SA}] = 10^6\,\mathrm{cm}^{-3}$. The small fraction of the SA–DMA clusters is to be expected at the higher DMA concentrations, as there are more DMA monomers than SA monomers in the simulated system. The simulations were performed at $T = 298.15\,\mathrm{K}$, where 1 ppt of DMA corresponds to $\sim 2.5 \times 10^7\,\mathrm{cm}^{-3}$ at a total pressure of 1 atm. Thus, for [DMA] = 100 ppt, $[\mathrm{SA}] = 10^8\,\mathrm{cm}^{-3}$ the DMA monomer concentration is roughly 1 order of magnitude larger than the concentration of SA monomers. The absence of larger neutral clusters in this figure results from the boundary conditions mentioned in Sect. 2 and does not imply they are not formed. However, in the paper by Almeida et al. (2013), the measured neutral SA dimer concentration (with likely 1–2 DMA molecules) was roughly 3–5 orders of magnitude lower than the corresponding DMA concentration. Thus, the exclusion of these and larger neutral clusters from the simulations should have a negligible effect on the results.

Figure 2 shows the time evolution of concentrations when protonated acetone dimers are introduced into the system. As stated earlier, the ionization time was set to 0.2 s, which is an estimate for the time the sample stays inside the ionization chamber in an acetone-CI-APi-TOF. Each subplot represents a combination of an initial SA concentration and an initial DMA concentration, with DMA concentration increasing from top to bottom and SA concentration increasing from left to right. The concentration of the charger ions has not been plotted in these figures.

Looking at the subplots in Fig. 2, we see two cluster types stand out. When [DMA] = 0.01 ppt, the main characteristic is a nearly linear increase in the concentration of $H^+(Ac)_1(DMA)_1$ clusters. These are mainly formed from collisions between $H^+(Ac)_2$ and $(DMA)_1$, resulting in a $H^+(Ac)_2(DMA)_1$ cluster, which then quickly evaporates an acetone monomer. In addition, some of the $H^+(Ac)_1(DMA)_1$ clusters are formed in collisions between the DMA monomers and $H^+(Ac)_1$. The end concentration of $H^+(Ac)_1(DMA)_1$ for [DMA] = 0.01 ppt depends on the SA concentration, nearly doubling for $[\mathrm{SA}] = 10^8\,\mathrm{cm}^{-3}$. This is because the $(SA)_1(DMA)_1$ cluster has a higher dipole moment than the uncharged DMA monomer, which leads to a higher collision frequency with the charger ions. Thus, if the relative concentration of $(SA)_1(DMA)_1$ clusters is significant, the overall charging efficiency is affected. When [DMA] = 100 ppt, we also see an increase of clusters with two dimethylamine molecules and a proton. These $H^+(DMA)_2$ clusters are mainly produced when a DMA molecule collides with a $H^+(Ac)_1(DMA)_1$ cluster, causing the acetone molecule to evaporate and resulting in a $H^+(DMA)_2$ cluster. A small fraction of these clusters is also produced in collisions between $H^+(DMA)_1$ and a DMA monomer. While increase of the $H^+(Ac)_1(DMA)_1$ cluster concentration slows down towards the 0.2 s mark, the concentration of the $H^+(DMA)_2$ clusters seems to exhibit a slightly accelerating growth. The sum of these two curves exhibits a nearly linear growth for all three cases. This indicates that – at least for the 0.2 s time period – the depletion of charger ions in the charging process does not significantly affect the rate at which $H^+(Ac)_1(DMA)_1$ is formed at this DMA concentration. When [DMA] = 3000 ppt, we see a quick initial increase of $H^+(Ac)_1(DMA)_1$ clusters followed by a decrease, finally resulting in a complete depletion of these clusters. The concentration of the $H^+(DMA)_2$ cluster initially increases slightly slower, but continues to grow until practically all the protons in the system have ended up in these clusters. For this DMA concentration, the charger ions are depleted already before 0.1 s of the ionization time has

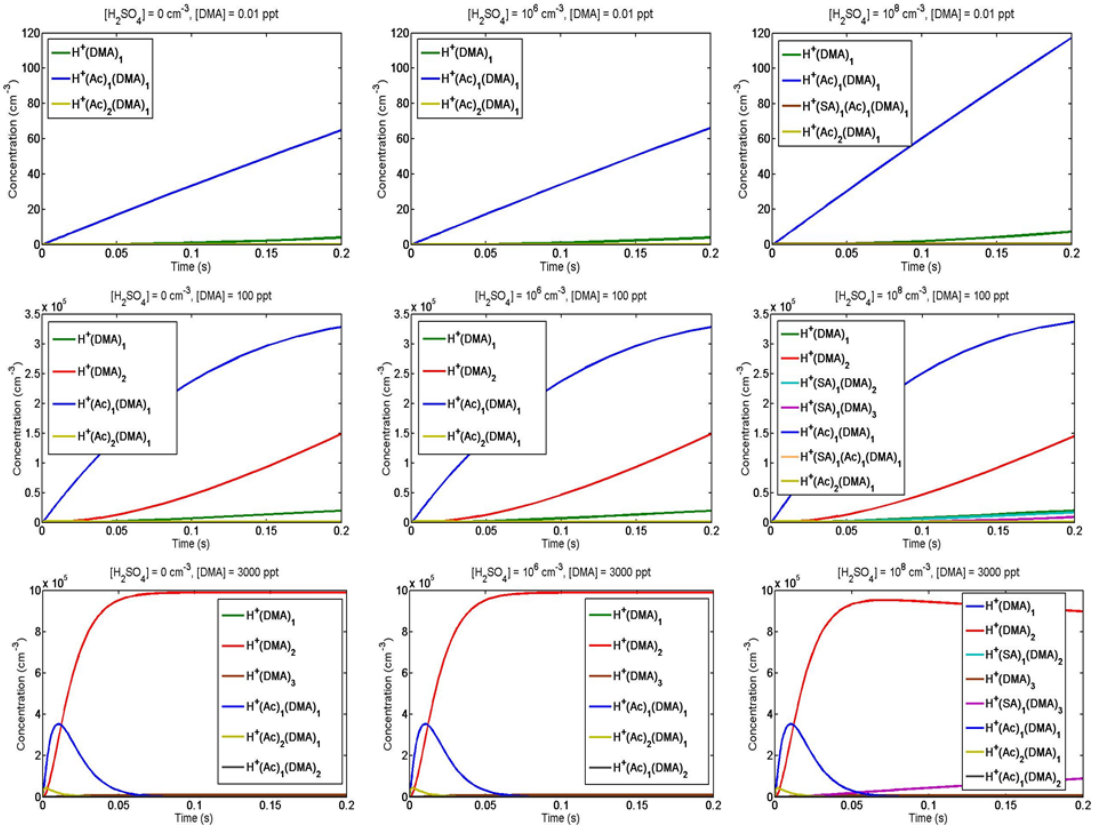

Figure 2. Modelled concentrations during chemical ionization. The columns are ordered from left to right by increasing sulfuric acid concentration, and the rows are ordered from top to bottom by increasing dimethylamine concentration. The temperature is 298.15 K in all subplots.

passed, as the sum of the concentrations plotted in the figure ceases to increase after reaching 10^6, which is the number of charger ions initially present (see bottom row of Fig. 2). The appearance of very small amounts of other cluster types not mentioned above can also be seen for all DMA concentrations.

The mechanism for the growth of the $H^+(DMA)_2$ concentration is rather simple: the higher the DMA concentration, the more collisions involving DMA there are. As the concentration of the $H^+(Ac)_1(DMA)_1$ clusters grows, so does the rate of collisions between a DMA molecule and a $H^+(Ac)_1(DMA)_1$ cluster. These collisions will result in a $H^+(DMA)_2$ cluster, plus an uncharged acetone molecule. Thus, given enough time and DMA monomers, all of the $H^+(Ac)_1(DMA)_1$ clusters will be transformed into $H^+(DMA)_2$ clusters. If the DMA concentration is high enough, this will happen very quickly, as can be seen for the case of [DMA] = 3000 ppt.

The concentrations of charged clusters after ionization are indicated by the end points of the different concentration curves in Fig. 2. This information is collected and presented in Figs. 3–5.

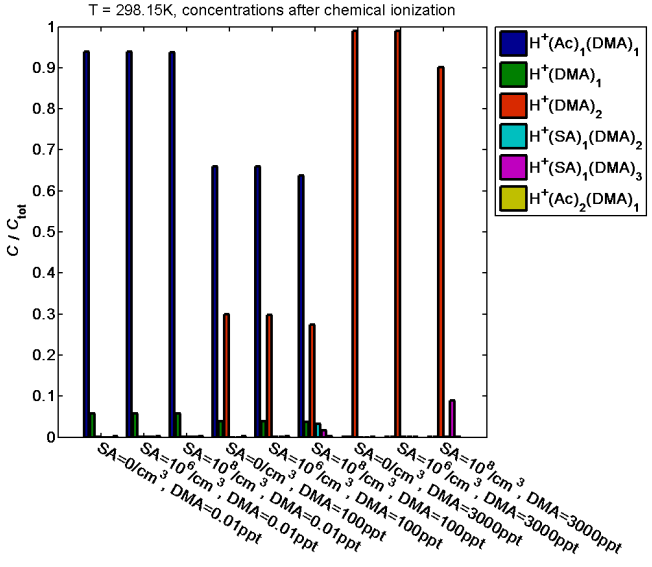

Figure 3. Relative concentrations of charged clusters after ionization grouped by cluster type.

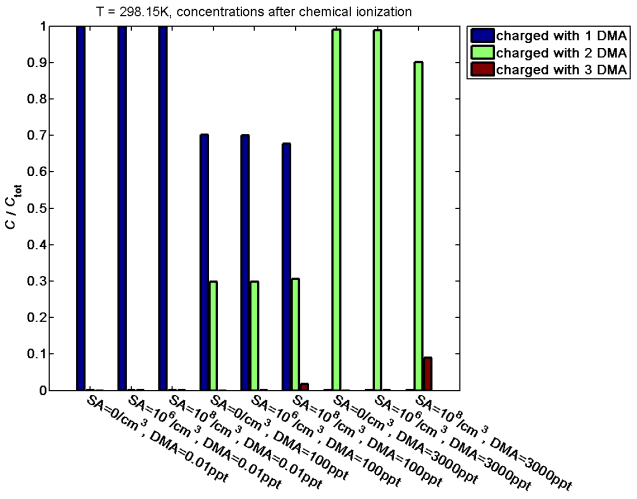

Figure 4. Relative concentrations after ionization grouped by the amount of DMA molecules in the cluster.

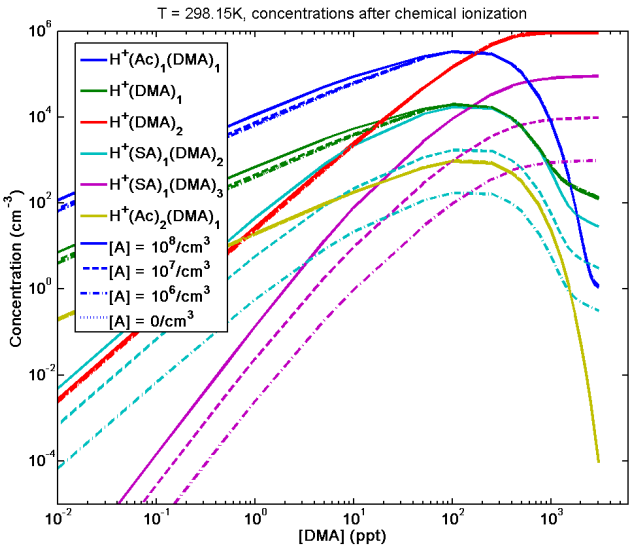

Figure 5. Modelled number concentrations of charged clusters after chemical ionization. The sticking factor was 1 for all collisions, the initial neutral acetone monomer concentration was 0 cm^{-3}, and the initial charger ion concentration was 10^6 cm^{-3}.

Figure 3 shows the relative concentration of different types of charged clusters after the chemical ionization. As can be seen, $H^+(Ac)_1(DMA)_1$ is clearly the most abundant charged cluster type for [DMA] = 0.01 ppt and [DMA] = 100 ppt. The fraction of $H^+(DMA)_1$ clusters does not depend on the SA concentration and is ∼5 % for [DMA] = 0.01 ppt, ∼4 % for [DMA] = 100 ppt and less than 1 % for [DMA] = 3000 ppt. In practice all of these clusters are formed when an acetone evaporates from an $H^+(Ac)_1(DMA)_1$ cluster. It should be noted that the ambient conditions in Hyytiälä would correspond roughly to [DMA] = 0.01 ppt (or more) and [SA] = 10^6 cm^{-3}. Thus, based on the ACDC results, a measurement performed on the ambient air should show mostly $H^+(Ac)_1(DMA)_1$ clusters with possibly small amounts of $H^+(DMA)_1$. At [DMA] = 100 ppt about a third of the clusters are of the type $H^+(DMA)_2$. When we have [DMA] = 100 ppt and [SA]=10^8 cm^{-3}, we also see small amounts of $H^+(SA)_1(DMA)_2$ clusters, which are mainly formed in collisions between $H^+(DMA)_2$ clusters and SA monomers or in collisions between $(SA)_1(DMA)_1$ and $H^+(Ac)_1(DMA)_1$ clusters (since it is assumed that the acetone molecule evaporates immediately). A fraction of these clusters is formed in collisions between $(SA)_1(DMA)_1$ and $H^+(DMA)$. Also small amounts of $H^+(SA)_1(DMA)_3$ clusters are seen at [DMA] = 100 ppt and [SA] = 10^8 cm^{-3}. These clusters are mainly formed in collisions between $(SA)_1(DMA)_1$ and $H^+(DMA)_2$ clusters. For [DMA] = 3000 ppt, the most abundant charged cluster type is $H^+(DMA)_2$, and only a negligible amount of other cluster types can be seen. The only exception is the $H^+(SA)_1(DMA)_3$ cluster, which form about 10 % of the cluster population when [SA] = 10^8 cm^{-3}.

The same data classified by the amount of DMA molecules in the clusters are shown in Fig. 4. As could already be deduced from Fig. 3, clusters containing one DMA dominate when [DMA] = 0.01 ppt and [DMA] = 100 ppt, with about a third of the clusters having 2 DMA molecules when [DMA] = 100 ppt and about 2 % of clusters having 3 DMA molecules when [DMA] = 100 ppt and [SA] = 10^8 cm^{-3}. For [DMA] = 3000 ppt, clusters having 2 DMA molecules dominate, with about 10 % of clusters having 3 DMA molecules, when [SA] = 10^8 cm^{-3}.

Figure 5 shows the number concentration of charged clusters as a function of the DMA concentration. Here [SA] was given values 0, 10^6, 10^7 and 10^8 cm^{-3}, while [DMA] was given several values between 0.01 and 3000 ppt. The colours correspond to cluster types, and the different types of lines correspond to different concentrations of SA. The $H^+(Ac)_1(DMA)_1$ cluster is the most abundant type up to about [DMA] = 200 ppt. After this point, the $H^+(DMA)_2$ cluster is the most abundant. For DMA concentrations of up to [DMA] = 100 ppt, the $H^+(DMA)_1$ cluster is more abundant than the $H^+(DMA)_2$ cluster, and for larger concentrations the situation is reversed. At high DMA concentrations the $H^+(SA)_1(DMA)_2$ and $H^+(SA)_1(DMA)_3$ clusters are the only cluster types the sulfuric acid concentration has a significant effect on. While the concentrations of these clusters are not generally very high, for [SA] = 10^8 cm^{-3} and [DMA] > 1000 ppt the $H^+(SA)_1(DMA)_3$ cluster has the second highest concentration. At low DMA concentrations the SA concentration has an effect on the charging efficiency, as was stated previously. The evaporation rates (order of magnitude accuracy) for the allowed cluster sizes are listed in Table 2.

The evaporation rates used in the simulation are obtained using the calculated changes in free energies. These are ex-

Table 2. The order of magnitudes of evaporation rates for the possible evaporation reactions for each cluster type that is formed in the simulation and is within the size limits presented in Table 1. The cluster types listed in Fig. 5 are marked with an asterisk (*).

Cluster	Calculated evaporation rate [1/s]
$H^+(Ac)_1(DMA)_1$*	$\sim 10^{-22}$ [$H^+(Ac)_1+(DMA)_1$] $\sim 10^{-1}$ [$H^+(DMA)_1+(Ac)_1$]
$H^+(DMA)_2$*	$\sim 10^{-2}$ [$H^+(DMA)_1+(DMA)_1$]
$H^+(SA)_1(DMA)_2$*	$\sim 10^{-15}$ [$H^+(SA)_1(DMA)_1+(DMA)_1$] $\sim 10^{-11}$ [$H^+(DMA)_1+(SA)_1(DMA)_1$] $\sim 10^{-10}$ [$H^+(DMA)_2+(SA)_1$]
$H^+(SA)_1(DMA)_3$*	$\sim 10^{-16}$ [$H^+(DMA)_3+(SA)_1$] $\sim 10^{-11}$ [$H^+(DMA)_2+(SA)_1(DMA)_1$] $\sim 10^{-2}$ [$H^+(SA)_1(DMA)_2+(DMA)_1$]
$H^+(Ac)_2(DMA)_1$*	$\sim 10^{-32}$ [$H^+(Ac)_1+(Ac)_1(DMA)_1$] $\sim 10^{-11}$ [$H^+(Ac)_2+(DMA)_1$] $\sim 10^{2}$ [$H^+(Ac)_1(DMA)_1+(Ac)_1$]
$(SA)_1(DMA)_1$	$\sim 10^{-1}$ [$(DMA)_1+(Ac)_1$]
$(Ac)_1(SA)_1$	$\sim 10^{7}$ [$(Ac)_1+(SA)_1$]
$(Ac)_1(DMA)_1$	$\sim 10^{13}$ [$(Ac)_1+(DMA)_1$]
$H^+(Ac)_2$	$\sim 10^{-8}$ [$H^+(Ac)_1+(Ac)_1$]
$H^+(Ac)_3$	$\sim 10^{8}$ [$H^+(Ac)_2+(Ac)_1$]
$H^+(DMA)_3$	$\sim 10^{3}$ [$H^+(DMA)_2+(DMA)_1$]
$H^+(SA)_1(DMA)_1$	$\sim 10^{2}$ [$H^+(DMA)_1+(SA)_1$]
$H^+(SA)_1(Ac)_2$	$\sim 10^{-8}$ [$H^+(Ac)_1+(SA)_1(Ac)_1$] $\sim 10^{7}$ [$H^+(Ac)_2+(SA)_1$]
$H^+(Ac)_1(DMA)_2$	$\sim 10^{-12}$ [$H^+(DMA)_1+(Ac)_1(DMA)_1$] $\sim 10^{2}$ [$H^+(Ac)_1(DMA)_1+(DMA)_1$] $\sim 10^{4}$ [$H^+(DMA)_2+(Ac)_1$]
$H^+(SA)_1(Ac)_1(DMA)_1$	$\sim 10^{-18}$ [$H^+(Ac)_1+(SA)_1(DMA)_1$] $\sim 10^{-6}$ [$H^+(DMA)_1+(Ac)_1(SA)_1$] $\sim 10^{-1}$ [$H^+(SA)_1(DMA)_1+(Ac)_1$] $\sim 10^{2}$ [$H^+(Ac)_1(DMA)_1+(SA)_1$]
$H^+(SA)_1(Ac)_2(DMA)_1$	$\sim 10^{-14}$ [$H^+(SA)_1(Ac)_2+(DMA)_1$] $\sim 10^{-5}$ [$H^+(Ac)_2+(SA)_1(DMA)_1$] ~ 1 [$H^+(Ac)_1(DMA)_1+(SA)_1(Ac)_1$] $\sim 10^{4}$ [$H^+(Ac)_2(DMA)_1+(SA)_1$] $\sim 10^{5}$ [$H^+(SA)_1(Ac)_1(DMA)_1+(Ac)_1$]

pected to be accurate to within a couple of kcal/mol for the simulated clusters. This can lead to some quantitative error, but qualitative results are expected to be correct. In addition to the cluster energies used in the simulations, higher-level benchmark calculations were performed for the DMA and acetone molecules and their protonated counterparts using the W1BD model chemistry method (Martin and de Oliveira, 1999; Barnes et al., 2009). The results for the Gibbs free energy and enthalpy of the proton transfer reaction $H^+(Ac)_1+(DMA)_1 \rightarrow (Ac)_1+H^+(DMA)_1$ are shown in Table 3. The table shows that a proton transfer reaction is predicted to be favourable regardless of the method, and the two methods give even quantitatively very similar results. Thus, our choice of quantum chemical method is not likely to introduce large errors in describing the proton transfer reaction. Rather than the reaction energetics, the other parameters used by the ACDC model (for example the sticking factors) are likely to be the major sources of errors in the modelling.

Table 3. The Gibbs free energy and enthalpy of the proton transfer reaction $H^+(Ac)_1+(DMA)_1 \rightarrow (Ac)_1+H^+(DMA)_1$.

	Gibbs free energy (kcal mol^{-1})	Enthalpy (kcal mol^{-1})
B3LYP/CBSB7/ /RI-CC2/aug-cc-pVTZ	−28.13	−28.11
W1BD	−27.50	−27.86

Based on the ACDC results, it seems clear that protonated acetone dimers can in principle be used to charge DMA molecules. A clear majority of the charged DMA-containing clusters are of the type $H^+(Ac)_1(DMA)_1$, but at high DMA concentrations most of these are expected to be converted into protonated DMA dimers. Before the ionization the simulated sample air also contained clusters of the type $(SA)_1(DMA)_1$ at high sulfuric acid. These clusters are mainly lost due to collisions with sulfuric acid monomers or neutral clusters with at least one sulfuric acid, in which case they grow out of the model system and are not considered further. Collisions with the charger ions result in $H^+(SA)_1(Ac)_2(DMA)_1$ clusters, which will quickly evaporate an acetone and a sulfuric acid (either one can evaporate first, but the evaporation of acetone is slightly more probable), resulting in a $H^+(Ac)_1(DMA)_1$ cluster. Collisions with $H^+(Ac)_1$, $H^+(DMA)_1$ and $H^+(DMA)_2$ are also possible and lead to $H^+(SA)_1(Ac)_1(DMA)_1$, $H^+(SA)_1(DMA)_2$ and $H^+(SA)_1(DMA)_3$ clusters, respectively. The first of these three cluster types will quickly evaporate the sulfuric acid, resulting in $H^+(Ac)_1(DMA)_1$, while the two other clusters are relatively stable, as can be seen from the evaporation rates in Table 2. The simulations demonstrate that the presence of large amounts of sulfuric acid significantly affects the concentration of H^+–DMA–Ac clusters only at low DMA concentrations. At higher DMA concentrations only the concentrations of clusters containing sulfuric acid are affected by the SA concentration. As the simulation does not consider, for example, wall losses, hydration or explicit molecule dynamics, the result should be considered qualitative.

The results are robust with respect to the various simplifications made in the simulations: for example, wall losses will affect only the quantitative results to some extent, but not the overall picture, and hydration is unlikely to prevent the proton transfer – instead, water molecules could in fact act as proton bridges. However, as Fig. 2 already implies, the time given for the charging can have an ef-

fect on the end result. Between the values 0.1, 0.15, 0.2, 0.25 and 0.3 s, there are some quantitative changes, but qualitative results stay the same: the $H^+(Ac)_1(DMA)_1$ clusters are the most abundant when [DMA] = 0.01 ppt and [DMA] = 100 ppt, while the $H^+(DMA)_2$ clusters are the most abundant when [DMA] = 3000 ppt. If the charging time is set to 0.01 s, the charger ions do not have enough time to collide with molecules in the sample air. This leads to a situation where the $H^+(Ac)_1(DMA)_1$ clusters are also the most abundant for [DMA] = 3000 ppt. Setting the charging time to 0.4 s we see a qualitative change only at [DMA] = 100 ppt, as the DMA molecules have enough time to collide with the $H^+(Ac)_1(DMA)_1$ clusters to produce $H^+(DMA)_2$ clusters, making them the most abundant cluster type. The implication that acetone can be used to charge DMA-containing clusters is unaffected regardless of the charging time. However, these comparisons serve as a healthy reminder of how quick the reactions relevant to charging are, and that changes of even fractions of a second in the allowed reaction times may be enough to change the measurement results noticeably. Increasing the amount of charger ions when DMA concentration is 0.01, 100 and 3000 ppt increases the absolute concentrations of all cluster types at the end of the ionization, as could be expected. Up to a charger ion concentration of 10^9 cm^{-3}, the relative concentrations of charged cluster species stay roughly the same. For the case of [DMA] = 0.01 ppt changes are small even beyond a charger ion concentration of 10^9 cm^{-3}. For the other two DMA concentrations changes are more notable, although qualitative changes can only be seen for [DMA] = 3000 ppt for which the $H^+(Ac)_1(DMA)_1$ cluster type becomes the most abundant at charger ion concentrations of 10^{11} and 10^{12} cm^{-3}. However, as was pointed out earlier, this high ion concentrations were used only to test the sensitivity and would not be present in a typical measurement.

The effect of using only protonated acetone dimers or protonated acetone monomers as charger ions was also tested for charger ion concentration of 10^6 cm^{-3} with [DMA] = 0.01 ppt, [DMA] = 100 ppt, [DMA] = 3000 ppt, [SA] = 0, [SA] = 10^6 cm^{-3} and [SA] = 10^8 cm^{-3}. While small quantitative changes could be seen in the absolute concentrations after ionization, the only qualitative change was seen in the concentration of the $H^+(Ac)_2(DMA)_1$ cluster type, as could be expected. The drop in absolute concentration after ionization, when changing from protonated acetone dimers to protonated acetone monomers, ranged roughly from 10 orders of magnitude (for [DMA] = 0.01 ppt) to 2 orders of magnitude (for [DMA] = 3000 ppt). Since this cluster type accounts for only a small portion of the total ion concentration excluding the charger ions, the relative concentrations of the charged cluster types were in practice identical for both charger ion types. When using only protonated acetone monomers as charger ions, the total ion concentrations were higher by ∼ 10–20 % and ∼ 5–10 % for [DMA] = 0.01 ppt and [DMA] = 100 ppt, respectively. For [DMA] = 3000 ppt the difference in total ion concentrations was negligible compared to the total ion concentrations obtained using only protonated acetone dimers as charger ions. The increase in total ion concentration for [DMA] = 0.01 ppt is due to the higher collision rate of the protonated acetone monomer. The increase becomes smaller for [DMA] = 100 ppt, since ∼ 50 % of the charger ions are depleted during ionization. For [DMA] = 3000 ppt in practice all of the charger ions are depleted regardless of which charger ion is used. Thus, the qualitative results are unaffected by which charger ion, or a combination of charger ion types is used in the simulations.

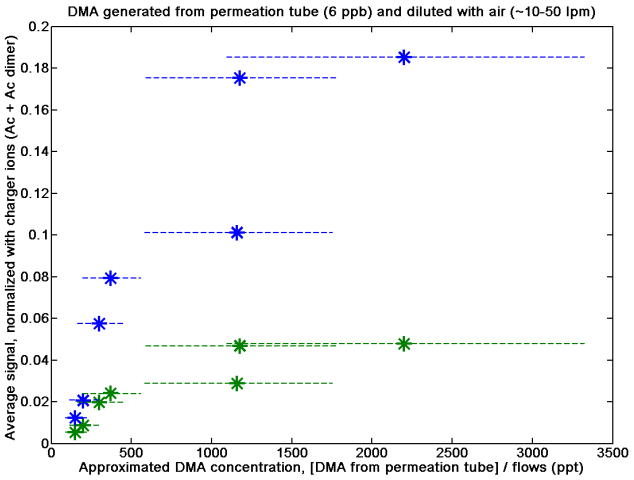

Figure 6. Measurement data from CI-APi-TOF, presented as the normalized average signals of ion counts per second. Green stars are for $H^+(DMA)_1$, and blue stars are for $H^+(Ac)_1(DMA)_1$. The error bars in the direction of the x axis are calculated using known sources of error and propagation of uncertainty. The error in the direction of the y axis is assumed to be negligible.

4 Comparison to experiments

The average signal in ion counts per second (cps) of the $H^+(Ac)_1(DMA)_1$ and $H^+(DMA)_1$ clusters measured by the CI-APi-TOF and normalized with the measured average signal in cps (after charging) of charger ions are presented in Fig. 6. The cps signals were not converted to concentrations at any point, as the values of the normalized cps signals should be similar to the normalized concentrations and quantitatively accurate values were not essential to the comparison. The signal peaks were clean with no interfering compounds present with the same mass. This is the main advantage in using chemical ionization and it demonstrates the usability of protonated acetone as reagent ion for base measurements. The error in the direction of the x axis is calculated using known sources for error (permeation rate and dilution) and propagation of uncertainty. On top of that there may be additional error sources, including any wall effects (adsorption/desorption), which are unknown but potentially large.

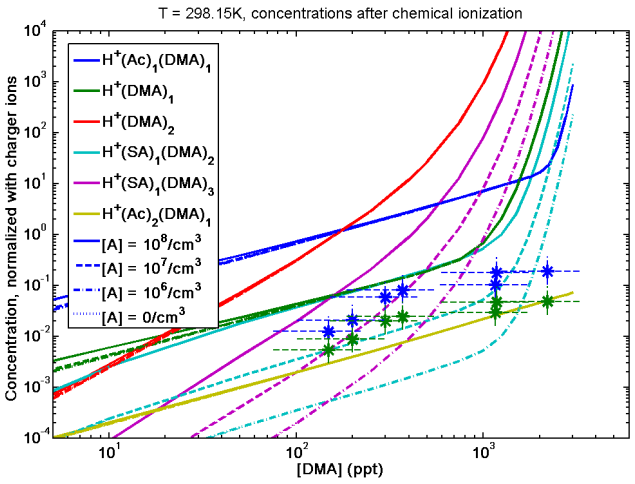

Figure 7. Modelled concentrations of charged clusters after chemical ionization, normalized with the remaining charger ion concentration after the ionization, ($[H^+(Ac)_1] + [H^+(Ac)_2]$). The sticking factor was 1 for all collisions, the neutral acetone monomer concentration was 0 cm^{-3}, and the initial charger ion concentration was 10^6 cm^{-3}. The stars represent the CI-APi-TOF measurement data, presented as the normalized average signals of ion counts per second. Green stars are for $H^+(DMA)_1$ and blue stars are for $H^+(Ac)_1(DMA)_1$. The error bars in the direction of the x axis are calculated using known sources of error and propagation of uncertainty. The error bars in the direction of the y axis represent the uncertainty in ion transmission coefficients.

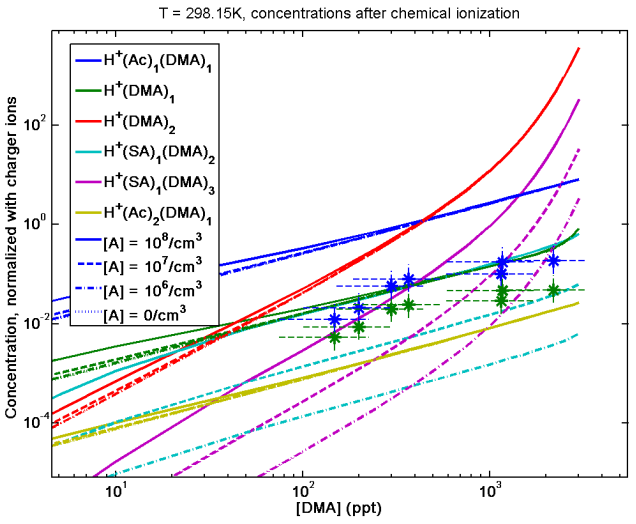

Figure 8. Modelled concentrations of charged clusters after chemical ionization, normalized with the remaining charger ion concentration after the ionization, ($[H^+(Ac)_1] + [H^+(Ac)_2]$). The sticking factor was 0.4 for collisions between DMA monomers and everything else, and 1 for all other collisions, the neutral acetone monomer concentration was 0 cm^{-3}, and the initial charger ion concentration was 10^6 cm^{-3}. The stars represent the CI-APi-TOF measurement data, presented as the normalized average signals of ion counts per second. Green stars are for $H^+(DMA)_1$ and blue stars are for $H^+(Ac)_1(DMA)_1$. The error bars in the direction of the x axis are calculated using known sources of error and propagation of uncertainty. The error bars in the direction of the y axis represent the uncertainty in ion transmission coefficients.

The error in the direction of the y axis is unknown. This is because the error in cps is very hard to estimate and also because the averaging hides the fluctuations in the signal, which could contain information of possible errors. However, any error in the average signal is assumed to be negligible compared to the magnitude of the averaged signal itself.

The figure shows that the signal for $H^+(Ac)_1(DMA)_1$ is higher than the signal for $H^+(DMA)_1$ regardless of the DMA concentration. In addition, the signal strength does not seem to grow linearly with growing DMA concentration, especially for the case of $H^+(Ac)_1(DMA)_1$. Instead, the increase seems to slow down, which is unexpected, as this might imply that some of the DMA is lost before it is charged. The change in the increase rate of the signal strength occurs between [DMA] = 500 ppt and [DMA] = 1000 ppt. The $H^+(DMA)_2$ cluster, which was the most abundant type in the modelling results after [DMA] = 200 ppt, was not observed in the measurements.

The data points are shown together with the normalized ACDC results in Fig. 7. In this figure – as well as in Figs. 8 and 9 – the data points also have error bars in the direction of the y axis. This is because the normalized ACDC values are based on exact modelled concentrations given as molecules per cubic centimetre, whereas the normalized measurement results are based on averaged cps. These are directly comparable only when the ion transmission coefficient is the same for all measured signals, in other words both measured clusters as well as both charger ions. This is likely not the case, as the ion transmission coefficient usually depends on the mass of the ion. Unfortunately, the transmission of the CI-APi-TOF is unknown for this measurement at the moment. Thus, we have used a conservative estimate of −50 %/+100 % for the error. However, depending on the transmission and memory effect it could be as large as −80 %/+400 %. The error bars in the direction of the x axis are the same as in Fig. 6 and reflect the fact that the DMA concentration in the measurement is an estimate based on the reported permeation rate of the DMA source and dilution. However, as was implied above, it is not well known how much of this DMA actually reaches the detector. Due to the error bars and related uncertainties, only the qualitative trends of the measurement data should be considered.

Looking at Fig. 7, we see that the difference in the simulated concentrations of $H^+(Ac)_1(DMA)_1$ and $H^+(DMA)_1$ clusters is larger than in the experimental concentrations of the same clusters. In addition, the DMA dependence of the experimental signal below [DMA] = 1000 ppt seems to be slightly stronger than that of the modelled concentrations. Above [DMA] = 1000 ppt, the last data point of the $H^+(Ac)_1(DMA)_1$ concentration, and the data points of the

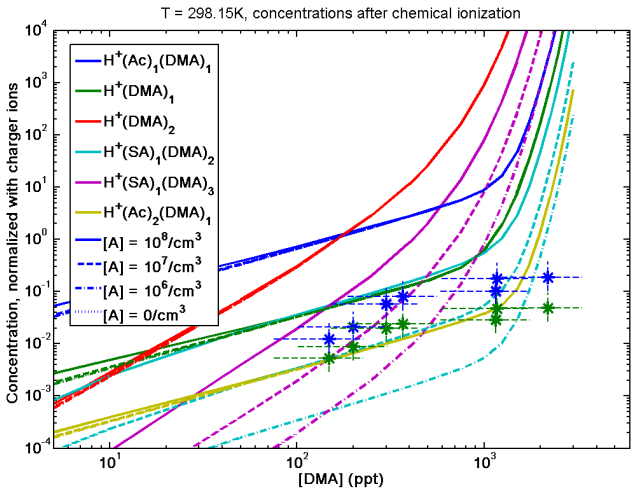

Figure 9. Modelled concentrations of charged clusters after chemical ionization, normalized with the remaining charger ion concentration after the ionization, ($[H^+(Ac)_1] + [H^+(Ac)_2]$). The sticking factor was 1 for all collisions, the neutral acetone monomer concentration was 10^9 cm^{-3}, and the initial charger ion concentration was 10^6 cm^{-3}. The stars represent the CI-APi-TOF measurement data, presented as the normalized average signals of ion counts per second. Green stars are for $H^+(DMA)_1$ and blue stars are for $H^+(Ac)_1(DMA)_1$. The error bars in the direction of the x axis are calculated using known sources of error and propagation of uncertainty. The error bars in the direction of the y axis represent the uncertainty in ion transmission coefficients.

$H^+(DMA)_1$ concentration do not follow the qualitative behaviour of the modelled concentrations. The upward "tail" in the modelled data is the result of the charger ions being depleted as the system becomes saturated with DMA. Similar behaviour can be observed in any measurement where the chemical species used for normalization is depleted, as could be expected. The "tail" should thus in principle also be observed experimentally for DMA at some concentration.

One possible explanation for this discrepancy is that the simulated "tail" is shifted to excessively low DMA concentrations. The reason for this could be that the formation rate of charged DMA clusters is lower than that predicted by the collision rates obtained with the used parameterization for ion-neutral collisions. Thus, possible steric effects were probed by tuning the sticking factor in the simulations. Lowering the sticking factor between DMA monomers and anything else results in lower concentrations for all cluster types as well as a shift in the "tail". A sticking factor of 0.4 is enough to shift the tail so that it does not show for the $H^+(Ac)_1(DMA)_1$ and $H^+(DMA)_1$ clusters at the experimentally studied DMA concentrations as can be seen in Fig. 8. Using this value yields similar behaviour for the modelled and the experimental concentrations, although the experimental $H^+(Ac)_1(DMA)_1$ concentrations remain an order of magnitude smaller than the modelled concentrations. On the other hand, the $H^+(DMA)_2$ cluster still has the "tail" in the simulations and becomes the most abundant cluster type at a DMA concentration of 500 ppt. As it is not detected in the CI-APi-TOF spectrum, it most likely either does not form or is fragmented in the APi. Thus the corresponding tail should be seen in one or both of the $H^+(Ac)_1(DMA)_1$ and $H^+(DMA)_1$ clusters.

In order to shift the location of the "tail" so that it does not show at the studied DMA concentrations for any cluster type, the sticking factor between DMA monomers and everything else would have to be roughly 0.2 or less. By further lowering the sticking factor, it is possible to lower the modelled concentrations so that the experimental data points for $H^+(Ac)_1(DMA)_1$ and $H^+(DMA)_1$ concentrations are between the curves of the modelled $H^+(Ac)_1(DMA)_1$ and $H^+(DMA)_1$ concentrations. Since the $H^+(DMA)_1$ cluster is mainly formed from the $H^+(Ac)_1(DMA)_1$ by evaporation of an acetone monomer, it is not possible to get the modelled concentrations of these clusters closer to each other just by tuning the sticking factor. While it is possible to further improve the agreement between the modelled and experimental concentrations by assigning different sticking factors for different collisions, there are no known physical grounds for choosing a specific value for any collision. Thus, tuning the sticking factors should only be considered an ad hoc solution, which, however, implies that steric effects may explain some of the mismatch between modelled and experimental concentrations.

The position of the "tail" of the acetone containing clusters is also affected by the neutral acetone monomer concentration. For the other cluster types the effect of neutral acetone is negligible. As can be seen from Fig. 9, setting the concentration of the neutral acetone monomers to 10^9 cm^{-3} instead of 0 cm^{-3} caused a notable change in the "tail" of $H^+(Ac)_1(DMA)_1$ and $H^+(Ac)_2(DMA)_1$ concentrations, which made the agreement between the simulated curves and the measurement points worse. This is somewhat unexpected, since while there are likely very few neutral acetone monomers among the charger ions, the ambient air in Hyytiälä used for dilution contained 10^{10}–10^{12} cm^{-3} of neutral acetone monomers. However, the measured concentrations agree best with modelled cases, where the neutral acetone monomer concentration is 10^7 cm^{-3} or less. Tuning the sticking factor of acetone monomers did not resolve the issue. Thus, the absence of neutral acetone monomers from the simulation results is not a realistic candidate for the discrepancy.

As the DMA concentrations in the experimental runs are estimations, another possible explanation for the discrepancy may be that the measurement points are positioned too far to the right in Fig. 7. In other words, the experimental DMA concentration might be overestimated, which could at least in part be due to wall and/or memory effects that are as yet unknown. However, the unexpected nonlinearity of the signal strength at low DMA concentrations in the measurements

is not resolved by a mere shift in the DMA concentrations, unless the error in the approximated DMA concentrations is dependent on the DMA concentration. Then again, the limited number of data points may also be the source of this discrepancy. In any case the charger ions do not seem to be as depleted in the measurement as they are in the simulations. A further discrepancy is that, according to the ACDC results, at the studied DMA concentrations significant amounts of $H^+(DMA)_2$ should also be seen by the CI-APi-TOF. Also $H^+(SA)_1(DMA)_3$ clusters should be observed at high sulfuric acid concentrations. While the sulfuric acid concentrations in the ambient air used for dilution in the measurements were always less than 10^7 cm^{-3}, the absence of $H^+(DMA)_2$ clusters is somewhat unexpected and gives reason to assume they are fragmented within the CI-APi-TOF. Other possible explanations are contamination or an isotope of the reagent ion with a similar mass, which would make detection harder. However, if these clusters do fragment, the result will most likely be a neutral DMA molecule and a $H^+(DMA)_1$ cluster, which may account for the fact that in the ACDC results the difference between the concentrations of $H^+(Ac)_1(DMA)_1$ and $H^+(DMA)_1$ is nearly 2 orders of magnitude, but in the measurements the difference is only about 1 order of magnitude. More importantly, if the $H^+(DMA)_2$ clusters fragment into a neutral DMA molecule and a $H^+(DMA)_1$ cluster, it would mean that a significant amount of the DMA present in the sample will not be observed in the measurement. Since there should be considerably more $H^+(DMA)_2$ to begin with than $H^+(DMA)_1$, a rough estimate is that the observed DMA concentration in the measurements is underestimating the true DMA concentration by an amount that corresponds to the observed concentration of $H^+(DMA)_1$. Looking at Fig. 4, this could translate into an error of ~ 20 %. However, before drawing such conclusions, the reason for the absence of the "tail" in the measured data needs to be explained.

5 Conclusions

Based on computational results, acetone is a viable option for use as a reagent ion in CI-APi-TOF measurements on atmospheric dimethylamine. However, there are notable discrepancies with the experimental and computational results. If chemical ionization happened at the collision limit as assumed by the simulations, the charger ions should get depleted at high DMA concentrations, but this is not observed in the measurements. Although the quantum chemical results concerning the thermodynamics of proton transfer are very likely robust, errors in the other simulation parameters can not be ruled out as a cause for the mismatch. In fact, the sticking factors (initially assumed to equal 1.0 for all collisions) likely play some role in the discrepancy. Including realistic concentrations of neutral acetone monomers in the simulations made the agreement with experimental results worse. Furthermore, the computational results suggest that at high DMA concentrations, the ionization process should produce high amounts of the cluster type $H^+(DMA)_2$. The fact that these have not been observed in the measurements could imply that, due to fragmentation within the CI-APi-TOF, observed DMA concentrations may underestimate the true DMA concentrations by 20 % or more. However, before the finding that the charger ions are not depleted as well as the absence of $H^+(DMA)_2$ in the measurement data is better understood, such estimations remain speculative. Also the role of neutral acetone in the measurements requires further investigation. Further study is still required before the acetone CI-APi-TOF can be considered a viable option in practice.

The Supplement related to this article is available online at doi:10.5194/amt-8-2577-2015-supplement.

Acknowledgements. We thank the CSC – IT Center for Science Ltd. for computer time and technical assistance. We also thank the TofTools team for providing tools for mass spectrometry data analysis. The financial support by the Academy of Finland (Centre of Excellence program Project No. 1118615, Research Fellow Project 1266388 and LASTU program project number 135054), Väisälä Foundation, PEGASOS project funded by the European Commission under the Framework Programme 7 (FP7-ENV-2010-265148) and ERC StG 257360-MOCAPAF is gratefully acknowledged.

Edited by: J. Schneider

References

Ahlrichs, R., Bär, M., Häser, M., Horn, H., and Kölmel C., Electronic Structure Calculations on Workstation Computers: The Program System TURBOMOLE, Chem. Phys. Lett., 162, 165, 1989.

Almeida, J., Schobesberger, S., Kürten, A., Ortega, I. K., Kupiainen-Määttä, O., Praplan, A. P., Adamov, A., Amorim, A., Bianchi, F., Breitenlechner, M., David, A., Dommen, J., Donahue, N. M., Downard, A., Dunne, E., Duplissy, J., Ehrhart, S., Flagan, R. C., Franchin, A., Guida, R., Hakala, J., Hansel, A., Heinritzi, M., Henschel, H., Jokinen, T., Junninen, H., Kajos, M., Kangasluoma, J., Keskinen, H., Kupc, A., Kurtén, T., Kvashin, A. N., Laaksonen, A., Lehtipalo, K., Leiminger, M., Leppä, J., Loukonen, V., Makhmutov, V., Mathot, S., McGrath, M. J., Nieminen, T., Olenius, T., Onnela, A., Petäjä, T., Riccobono, F., Riipinen, I., Rissanen, M., Rondo, L., Ruuskanen, T., Santos, F. D., Sarnela, N., Schallhart, S., Schnitzhofer, R., Seinfeld, J. H., Simon, M., Sipilä, M., Stozhkov, Y., Stratmann, F., Tomé, A., Tröstl, J., Tsagkogeorgas, G., Vaattovaara, P., Viisanen, Y., Virtanen, A., Vrtala, A., Wagner, P. E., Weingartner, E., Wex, H., Williamson, C., Wimmer, D., Ye, P., Yli-Juuti, T., Carslaw, K. S., Kulmala, M., Curtius, J., Baltensperger, U., Worsnop, D. R.,

Vehkamäki, H., and Kirkby, J.: Molecular understanding of sulphuric acid–amine particle nucleation in the atmosphere, Nature, 502, 359–363, doi:10.1038/nature12663, 2013.

Barnes, E. C., Petersson, G. A., Montgomery Jr., J. A., Frisch, M. J., and Martin, J. M. L.: Unrestricted Coupled Cluster and Brueckner Doubles Variations of W1 Theory, J. Chem. Theory Comput., 5, 2687–2693, 2009.

Frisch, M. J., Trucks, G. W., Schlegel, H. B., Scuseria, G. E., Robb, M. A., Cheeseman, J. R., Scalmani, G., Barone, V., Mennucci, B., Petersson, G. A., Nakatsuji, H., Caricato, M., Li, X., Hratchian, H. P., Izmaylov, A. F., Bloino, J., Zheng, G., Sonnenberg, J. L., Hada, M., Ehara, M., Toyota, K., Fukuda, R., Hasegawa, J., Ishida, M., Nakajima, T., Honda, Y., Kitao, O., Nakai, H., Vreven, T., Montgomery, Jr., J. A., Peralta, J. E., Ogliaro, F., Bearpark, M., Heyd, J. J., Brothers, E., Kudin, K. N., Staroverov, V. N., Kobayashi, R., Normand, J., Raghavachari, K., Rendell, A., Burant, J. C., Iyengar, S. S., Tomasi, J., Cossi, M., Rega, N., Millam, J. M., Klene, M., Knox, J. E., Cross, J. B., Bakken, V., Adamo, C., Jaramillo, J., Gomperts, R., Stratmann, R. E., Yazyev, O., Austin, A. J., Cammi, R., Pomelli, C., Ochterski, J. W., Martin, R. L., Morokuma, K., Zakrzewski, V. G., Voth, G. A., Salvador, P., Dannenberg, J. J., Dapprich, S., Daniels, A. D., Farkas, O., Foresman, J. B., Ortiz, J. V., Cioslowski, J., and Fox, D. J.: Gaussian 09, Revision A.01, Gaussian, Inc., Wallingford CT, 2009.

Junninen, H., Ehn, M., Petäjä, T., Luosujärvi, L., Kotiaho, T., Kostiainen, R., Rohner, U., Gonin, M., Fuhrer, K., Kulmala, M., and Worsnop, D. R.: A high-resolution mass spectrometer to measure atmospheric ion composition, Atmos. Meas. Tech., 3, 1039–1053, doi:10.5194/amt-3-1039-2010, 2010.

Jokinen, T., Sipilä, M., Junninen, H., Ehn, M., Lönn, G., Hakala, J., Petäjä, T., Mauldin III, R. L., Kulmala, M., and Worsnop, D. R.: Atmospheric sulphuric acid and neutral cluster measurements using CI-APi-TOF, Atmos. Chem. Phys., 12, 4117–4125, doi:10.5194/acp-12-4117-2012, 2012.

Kulmala, M., Kontkanen, J., Junninen, H., Lehtipalo, K., Manninen, H. E., Nieminen, T., Petäjä, T., Sipilä, M., Schobesberger, S., Rantala, P., Franchin, A., Jokinen, T., Järvinen, E., Äijälä, M., Kangasluoma, J., Hakala, J., Aalto, P. P., Paasonen, P., Mikkilä, J., Vanhanen, J., Aalto, J., Hakola, H., Makkonen, U., Ruuskanen, T., Mauldin III, R. L., Duplissy, J., Vehkamäki, H., Bäck, J., Kortelainen, A., Riipinen, I., Kurtén, T., Johnston, M. V., Smith, J. N., Ehn, M., Mentel, T. F., Lehtinen, K. E. J., Laaksonen, A., Kerminen, V.-M., and Worsnop, D. R.: Direct observations of atmospheric aerosol nucleation, Science, 22, 943–946, 2013.

Martin, J. M. L. and de Oliveira, G.: Towards standard methods for benchmark quality ab initio thermochemistry – W1 and W2 theory, J. Chem. Phys., 111, 1843–1856, 1999.

Kupiainen-Määttä, O., Olenius, T., Kurtén, T., and Vehkamäki, H.: CIMS sulfuric acid detection efficiency enhanced by amines due to higher dipole moments: a computational study, J. Phys. Chem. A, 117, 14109–14119, 2013.

Kyrö, E.-M., Kerminen, V.-M., Virkkula, A., Dal Maso, M., Parshintsev, J., Ruíz-Jimenez, J., Forsström, L., Manninen, H. E., Riekkola, M.-L., Heinonen, P., and Kulmala, M.: Antarctic new particle formation from continental biogenic precursors, Atmos. Chem. Phys., 13, 3527–3546, doi:10.5194/acp-13-3527-2013, 2013.

Loukonen, V., Kuo, I-F. W., McGrath, M. J., and Vehkamäki, H.: On the stability and dynamics of (sulfuric acid)(ammonia) and (sulfuric acid)(dimethylamine) clusters: a first-principles molecular dynamics investigation, Chem. Phys., 428, 164–174, 2014.

Ortega, I. K., Kupiainen, O., Kurtén, T., Olenius, T., Wilkman, O., McGrath, M. J., Loukonen, V., and Vehkamäki, H.: From quantum chemical formation free energies to evaporation rates, Atmos. Chem. Phys., 12, 225–235, doi:10.5194/acp-12-225-2012, 2012.

Ortega, I. K., Olenius, T., Kupiainen-Määttä, O., Loukonen, V., Kurtén, T., and Vehkamäki, H.: Electrical charging changes the composition of sulfuric acid-ammonia/dimethylamine clusters, Atmos. Chem. Phys., 14, 7995–8007, doi:10.5194/acp-14-7995-2014, 2014.

Petäjä, T., Sipilä, M., Paasonen, P., Nieminen, T., Kurtén, T., Ortega, I. K., Stratmann, F., Vehkamäki, H., Berndt, T. and Kulmala, M.: Experimental observation of strongly bound dimers of sulfuric acid: application to nucleation in the atmosphere, Phys. Rev. Lett. 106, 228302, doi:10.1103/PhysRevLett.106.228302, 2011.

Puton, J., Nousiainen, M., and Sillanpää, M.: Ion mobility spectrometers with doped gases, Talanta, 76, 978–987, 2008.

Sipilä, M., Berndt, T., Petäjä, T., Brus, D., Vanhanen, J., Stratmann, F., Patokoski, J., Mauldin III, R. L., Hyvärinen, A.-P., Lihavainen, H., and Kulmala, M.: The role of sulfuric acid in atmospheric nucleation, Science, 327, 1243–1246, 2010.

Su, T. and Chesnavich, W. J.: Parameterization of the ion-polar molecule collision rate constant by trajectory calculations, J. Chem. Phys., 76, 5183–5185, doi:10.1063/1.442828, 1982.

Yu, H. and Lee, S.-H.: Chemical ionisation mass spectrometry for the measurement of atmospheric amines, Environ. Chem., 9, 190–201, 2012.

Zhang, R., Khalizov, A., Wang, L., Hu, M., and Xu, W.: Nucleation and growth of nanoparticles in the atmosphere, Chem. Rev., 112, 1957–2011, 2012.